Fabrication of extracellular matrix-like membranes for loading piezoelectric nanoparticles

JPhys Materials

PAPER • OPEN ACCESS

Fabrication of extracellular matrix-like membranes for loading piezoelectric nanoparticles

To cite this article: Michela Licciardello *et al* 2020 *J. Phys. Mater.* **3** 034004

IOP Publishing J. Phys. Mater. 3 (2020) 034004 https://doi.org/10.1088/2515-7639/ab8572

Journal of Physics: Materials

OPEN ACCESS

RECEIVED
17 December 2019

REVISED
10 March 2020

ACCEPTED FOR PUBLICATION
1 April 2020

PUBLISHED
12 May 2020

PAPER

Fabrication of extracellular matrix-like membranes for loading piezoelectric nanoparticles

Michela Licciardello[1,2], Chiara Tonda-Turo[1,2], Andrea Gallina[1], Gianni Ciofani[3] and Gianluca Ciardell[1,2]

[1] Department of Mechanical and Aerospace Engineering, Politecnico di Torino, Turin, Italy
[2] POLITO BIOMedLAB, Politecnico di Torino, Turin, Italy
[3] Italian Institute of Technology, Smart Bio-Interfaces, Pontedera (Pisa), Italy

E-mail: chiara.tondaturo@polito.it

Keywords: piezoelectric membranes, electrospinning, tissue engineering, gelatin

Abstract

Piezoelectric ceramic nanomaterials have recently attracted attention in the biomedical field thanks to their interesting electrical properties in response to mechanical stimulation (and vice versa) combined with a good biocompatibility and the ability to promote the regeneration of electrically sensitive tissues. In tissue engineering approaches, in order to obtain smart scaffolds these materials must be combined with other biomaterials for processing through conventional as well as non-conventional technologies. In this work, a novel composite electrospun membrane was produced by combining extracellular matrix-like gelatin nanofibers with barium titanate nanoparticles (BTNPs). The electrospinning process was optimized to achieve a high BTNP load, reducing the formation of aggregates which could alter the morphology and stability of the membrane. A complete morphological, mechanical and chemical–physical characterization of the composite membranes was performed, confirming the integration of the BTNPs into the polymer fibers. Furthermore, the biocompatibility of the developed membranes was assessed using a sarcoma osteogenic cell line (SaOS-2).

1. Introduction

In the 20th century, tissue engineering was proposed as an innovative interdisciplinary field 'that applies the principles of biology and engineering to the development of functional substitutes for damaged tissue' (Langer and Vacanti 1993). One of the more attractive aims of tissue engineering is the fabrication of functional biological substitutes that can be implanted when the original tissue has been damaged (O'Brien 2011). A scaffold is the fundamental element on which tissue engineering approaches are based, and it acts as a template to temporarily replace the native extracellular matrix (ECM) and support cell growth and tissue regeneration (Jones 2005). In the physiological environment cells interact with the ECM through morphological, compositional and physical means as well as soluble cues. Nanofibrous scaffolds promote cell adhesion as they exhibit an architecture similar to native ECM, and the high surface/volume ratio, porosity and pore interconnection that characterizes nanofibrous scaffolds ensure the activation of different cellular processes such as cell proliferation and differentiation (Ng *et al* 2012, Paim *et al* 2018). Electrospinning is the most versatile and simple technique for obtaining nanofibrous mats for tissue engineering applications (Vasita and Katti 2006). A great advantage of this technique is its capability to process a large variety of materials, including natural polymers such as polysaccharides and proteins, which mimic the composition of the natural components of the ECM (Sell *et al* 2010) and are widely used in tissue engineering applications (Gupta *et al* 2014) thanks to their bioactivity and biocompatibility (Akilbekova *et al* 2018). Nanofibrous scaffolds obtained by electrospinning of natural polymers have been reported as a promising method for improving the regeneration of peripheral nerve (Rajabi *et al* 2018), skin (Pezeshki-Modaress *et al* 2018) and bone (Sisson *et al* 2010) tissue.

The electrospinning of natural polymers allows both the composition and the structure of the ECM to be mimicked; however, recent literature has highlighted the role of additional cues in enhancing new tissue

formation by inducing cell differentiation, migration and multicellular organization (Hofmann and Garcia-Fuentes 2011, Kesireddy and Kasper 2016). Some cell types have been reported to need additional cues which can direct and enhance tissue growth. Therefore, in recent years, the use of new smart materials has been investigated for tissue engineering applications (Ravichandran *et al* 2012). Among others, piezoelectric materials have been used; these materials have the ability to produce electrical activity in response to mechanical deformation without the need for an external source (Rajabi *et al* 2015). Piezoelectric ceramic nanomaterials with a perovskite-like structure, such as barium titanate ($BaTiO_3$) and lead zirconate ceramics (PZTs), have attracteded considerable attention from biomedical scientists for their interesting electrical properties combined with good biocompatibility (Dubey *et al* 2010, 2019, Wen and Liu 2014). Barium titanate nanoparticles (BTNPs) have often been used, alone or in combination with other biomaterials, to promote the regeneration of electrically sensitive tissues such as bone (Beloti *et al* 2006, Baxter *et al* 2010, Genchi and Marino *et al* 2016) and nerve (Marino *et al* 2015, Genchi and Ceseracciu *et al* 2016).

So far, composite electrospun polymeric membranes have been fabricated by combining BTNPs with a biocompatible synthetic polymer to form composite nanofibers. For instance, BTNPs were dispersed in polymeric solutions to confer dielectric behavior on electrospun mats, namely polycaprolactone (PCL)/BTNPs (Bagchi *et al* 2014) and poly(l -lactic acid) (PLLA)/BTNPs (Li *et al* 2017), but also to improve the properties of piezoelectric polymers such as poly(vinylidene fluoride-*co*-trifluoroethylene) [P(VDF-TrFE)]–$BaTiO_3$ (Genchi and Ceseracciu *et al* 2016)). These synthetic polymers did not supply haptotactic cues, which are key elements in cell adhesion and proliferation, thus reducing the biomimeticity of the final constructs.

Here, for the first time, we propose a method to produce ECM-like nanofibers with piezoelectric behavior by loading piezoelectric BTNPs into ECM-like natural polymer (gelatin, GL) electrospun membranes adopting a cell- and environmentally friendly protocol. The electrospinning protocol was optimized starting from the well-established method proposed by Tonda-Turo and colleagues (Tonda-Turo *et al* 2013, Marino *et al* 2017, Gnavi *et al* 2018) to fabricate homogeneous nanofibers. Gum arabic (GA), a neutral or low-acid water-soluble heteropolysaccharide, was added to an aqueous solution of BTNPs and GL to improve the dispersion of BTNPs in GL solution and reduce the size of the nanoparticle aggregates in the nanofibers. The viscosity of several solutions was studied thought rheological analysis. Nanofiber morphology was evaluated by scanning electron microscopy (SEM) and the BTNP content in GL mats was confirmed by energy dispersive x-ray spectroscopy (EDX) and thermogravimetric analysis (TGA). The mechanical properties of mats were measured by tensile testing. Finally, the biocompatibility of GL/BTNPs and the behavior of a sarcoma osteogenic cell line (SaOS-2) on the composite substrate were evaluated using the resazurin cell viability assay. Furthermore, preliminary tests were performed to assess the osteogenic potential of these substrates on mesenchymal stem cells (MSCs).

2. Materials and methods

2.1. Fabrication of electrospun mats

2.1.1. Preparation of GL/BTNP solutions.

GL (type A from porcine skin) and γ-glycidoxypropyltrimethoxysilane (GPTMS) were supplied by Sigma Aldrich, while BTNPs (300 nm) were purchased from Nanostructured & Amorphous Materials, Inc. Several composite solutions were prepared by varying the amount of BTNPs in the GL solution. Briefly, nanoparticle dispersions were obtained by sonicating solutions of BTNPs at different concentrations (10% w/v to 30% w/v with respect to the volume of GL solution) in double-distilled water for 20 min. GL (15% w/v) was added to the BTNP solution at 50 °C. After complete dissolution of GL, GPTMS crosslinker (92 μl g^{-1} GL) was added as reported by Tonda-Turo *et al* (2013). A GL solution without BTNPs was also prepared as a control according to Tonda-Turo *et al* (2013).

2.1.2. Optimization of BTNP dispersion.

In order to improve the dispersion of nanoparticles in the polymeric solution, GA (Sigma Aldrich) was dispersed in double-distilled water before adding BTNPs at concentrations of 10% w/v and 30% w/v. Two GA:BTNP weight ratios were tested: (a) 1:1 and (b) 2:1.

2.1.3. Rheological characterization of the solutions.

The rheological properties of several solutions were investigated with a MCR320 Anton Paar rheometer equipped with two parallel plane plates of 50 mm. A viscosity rotational test was carried out in order to study the influence of the GA and BTNP concentration on the viscosity of the solutions. The test was performed by putting 2 ml of any sample on the bottom plate of the rheometer under isothermal conditions at 50 °C; the

gap between the plates was 0.8 mm. The solution viscosity was obtained as a function of shear rate, which ranged from 0.1 to 100 s^{-1}.

2.1.4. Electrospinning of nanofibrous membranes.
In this work we used an electrospinning system in horizontal configuration supplied by Linari Engineering s.r.l. (figure S1 in the supplementary material, available at https://stacks.iop.org/JPMATER/3/034004/mmedia). Composite solutions were loaded into a 5 ml plastic syringe with a 21 G needle. The syringe was placed into a syringe pump to deliver the solution at a constant flow rate. A high voltage was applied between the syringe needle and a plane collector. The following electrospinning parameters were set: temperature 50 °C; voltage 30 kV; solution flow rate 1.5 ml h^{-1}; distance between needle and collector 12 cm. The electrospun samples was coded as GL (pure gelatin), GL/BTNPs 10 and GL/BTNPs 30 (10% w/v and 30% w/v of BTNPs in solution, respectively), and GL/BTNPs 10 GA and GL/BTNPs 30 GA (10% w/v and 30% w/v of BTNPs in solution, respectively, with optimized concentration of GA).

2.2. Characterization of the composite membranes
2.2.1. Scanning electron microscopy and energy dispersive x-ray analysis.
The morphological characterization of the electrospun samples was performed by SEM (LEO 435) with an accelerating voltage of 20 kV. Elemental analysis of the membrane was evaluated by EDX. Before SEM-EDX analysis, the samples were cut into squares of about 1 cm^2 and then sputtered with gold for 50 s at 30 mA under an Agar Auto Sputter Coater. The SEM images were analysed through ImageJ software (National Institutes of Health, USA) in order to quantify the fibers and the size of the BTNP aggregates. Fifty measures per sample were recorded; the average and standard deviation of the fiber diameters were calculated and reported.

2.2.2. Fourier transform infrared-attenuated total reflectance spectroscopy.
The chemical behavior of nanofibrous membranes was evaluated under a Fourier transform infrared-attenuated total reflectance (FTIR-ATR) spectroscope (Perkin Elmer) using diamond as the ATR crystal and the following conditions: wavenumber range 4000–800 cm^{-1}; resolution 4 cm^{-1}; number of scans 16. The sample spectra were analyzed and compared using Spectrum software .

2.2.3. Thermogravimetric analysis.
TGA was used to determinate the nanoparticle content in the electrospun membrane. The analysis was performed with a Mettler Toledo TGA apparatus in a temperature range of 30–800 °C with a heating flow of 10 °C min^{-1}. The samples were cut, giving small pieces of 5.4904 mg, 6.3403 mg and 6.2508 mg, respectively, for GL, GL/BTNPs 10 GA and GL/BTNPs 30 GA. After the analysis, the final weight of the samples was calculated from the residual percentage weight.

2.2.4. Mechanical characterization.
Mechanical tests were performed with a MTS QTest™/10 uniaxial tensile apparatus (figure S2) equipped with a fixed lower crossbar and an upper mobile crossbar. The mobile crossbar was connected to a load cell of 10 N and a displacement speed of 2 mm min^{-1} was set. Before the test, the samples were cut into rectangular pieces and their height, width and thickness measured; then they were loaded into the grips connected to the crossbars. At the end of the test, the stress–stain curve of the samples was determined and the Young's modulus (E), ultimate tensile strength (UTS) and strain at failure (ε%) were calculated (mean and standard deviation).

2.2.5. Cell viability assay: indirect tests.
The cytocompatibility of the composite membranes was evaluated by the culture of SaOS-2 cells on several substrates. The electrospun membranes were cut into small pieces and placed on the bottom of each well though CellCrown™ inserts (Sigma Aldrich). For each sample, 20×10^3 cells cm^{-2} were seeded and cultured with Dulbecco's modified Eagle's medium (DMEM; Sigma Aldrich) for 2 and 7 d on the substrates.

The resazurin assay was performed to evaluate cell viability using the metabolic capacity of viable cells to reduce non-fluorescent resazurin into fluorescent resorufin. Resazurin 10× was obtained by dissolving resazurin powder (1 mg ml^{-1}) in MilliQ water. Three samples for each condition were incubated with 1 ml of resazurin (1:10 in DMEM) for 1 h. The emission at 590 nm was detected by a multimode plate reader (VICTOR X3, Perkin Elmer) using 530 nm wavelength excitation. Measured values were compared with controls to assess the viability of composite membranes.

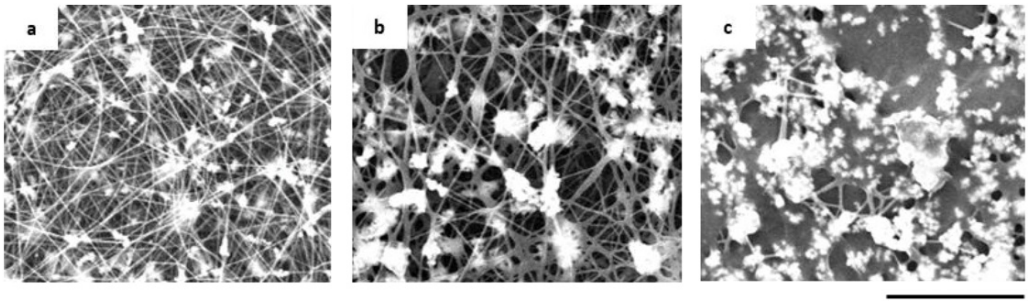

Figure 1. SEM images of GL/BTNP membranes (scale bar = 10 μm) with increasing BTNP concentration: (a) GL/BTNPs 10 (10% w/v of BTNPs in solution); (b) GL/BTNPs 20 (20% w/v of BTNPs in solution); (c) GL/BTNPs 30 (30% w/v of BTNPs in solution).

2.2.6. Osteogenic differentiation of MSCs.
Bone marrow-derived MSCs (ATCC-PCS-500-012) were cultured using MSC basal medium as suggested by the supplier. Three samples for each type of electrospun fiber were glued on 12 mm glass coverslips. Cells were seeded on the top of the nanofibrous mats at a density of 20×10^3 cells cm^{-2} and incubated for 7 d. Then alkaline phosphatase (ALP; Sigma Aldrich) and alizarin red (EMP Millipore) assays were performed to measure early osteogenic differentiation and to detect calcium deposition, respectively. For the ALP assay samples were fixed in formalin-free tissue fixative (Sigma Aldrich). Alkalization was measured using a plate reader (Victor X3, Perkin Elmer) at 405 nm and normalized for the number of cells measured with resazurin assay, as described in section **2.2.5**. For alizarin red, samples were fixed in formalin-free tissue fixative and stained with 1 ml of alizarin red solution for 30 min at room temperature. Then samples were washed in deionized water, dried overnight at 60 °C and observed under an optical microscope (Leica Biosystems). Experiments were repeated in triplicate.

2.2.7. Statistical analysis.
GraphPad Prism 8.2.1 was used for statistical analysis. A *t*-test was performed to compare two data class while ordinary one-way analysis of variance (ANOVA) was used to compare multiple groups.

3. Results

3.1. Protocol for optimization of solutions

3.1.1. Morphological characterization of GL/BTNP membranes.
GL/BTNP mats (coded as GL/BTNPs 10, GL/BTNPs 20 and GL/BTNPs 30) were fabricated by electrospinning of composite suspensions prepared as described in section **2.1.1**. The obtained membranes were morphologically characterized by SEM analysis. GL/BTNPs 10 and GL/BTNPs 20 (figures 1(a) and (b)) showed nanofibrous structures in a random configuration where the BTNPs were not uniformly distributed in the fibers but formed large aggregates. Conversely, GL/BTNPs 30 appeared to consist of a fibrous structure but was covered by a compact layer of polymer and nanoparticle aggregates.

3.1.2. Optimization of the GA:BTNP ratio.
To improve nanoparticle dispersion, GA was added to the aqueous solution before adding the BTNPs. The GA:BTNP ratio ranged from 1:1 (w/w) to 2:1 (w/w) to define the concentration that allowed us to obtain a uniform distribution of BTNPs in the fibers and reduce aggregate size. The effect of GA and BTNPs on the spinnability of the solutions was studied by comparing the viscosity of the various solutions. The trends of the curves showed non-Newtonian behavior of all the solutions (figures 2(a) and (b)). Furthermore, an increase in viscosity was observed corresponding to the increment in GA and BTNP concentration in the solution. The high viscosity of the solution with a 2:1 GA:BTNP ratio (w/w) hindered the spinnability of the solution. Thus, the GA:BTNP ratio was set to 1:1 (w/w). The procedure for the preparation of optimized solutions is shown schematically in figure S3.

3.2. Characterization of composite membranes

3.2.1. Morphological characterization.
GL and composite mats (coded as GL/BTNPs 10 GA and GL/BTNPs 30 GA) were obtained by electrospinning of solutions under the same electrospinning parameters reported in section **2.1.2**. SEM images of electrospun membranes (figure 3) showed a fibrous architecture in a random configuration in which the fiber size was 179 ± 46 nm, 230 ± 50 nm and 444 ± 97 nm for GL, GL/BTNPs 10 GA and

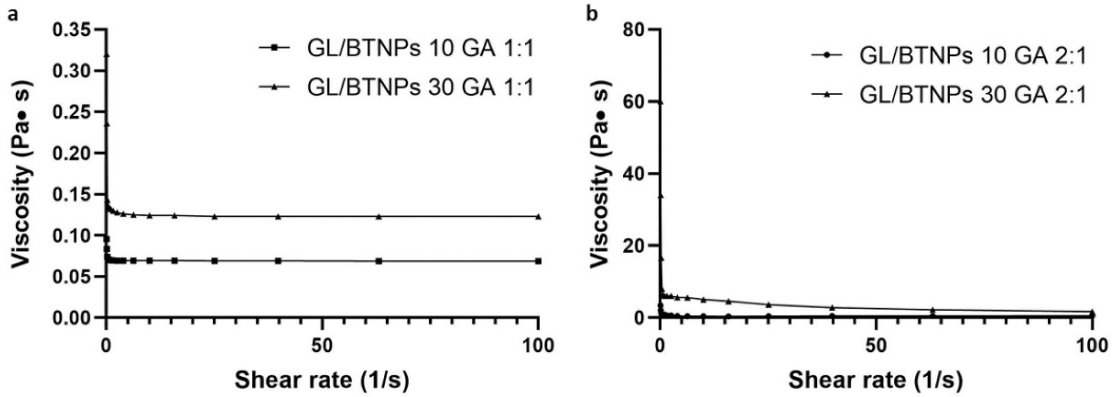

Figure 2. Viscosity trend as a function of shear rate for: (a) GL/BTNPs 10 and GL/BTNPs 30 with a GA:BTNP weight ratio of 1:1; (b) GL/BTNPs 10 and GL/BTNPs 30 with a GA:BTNP weight ratio of 2:1.

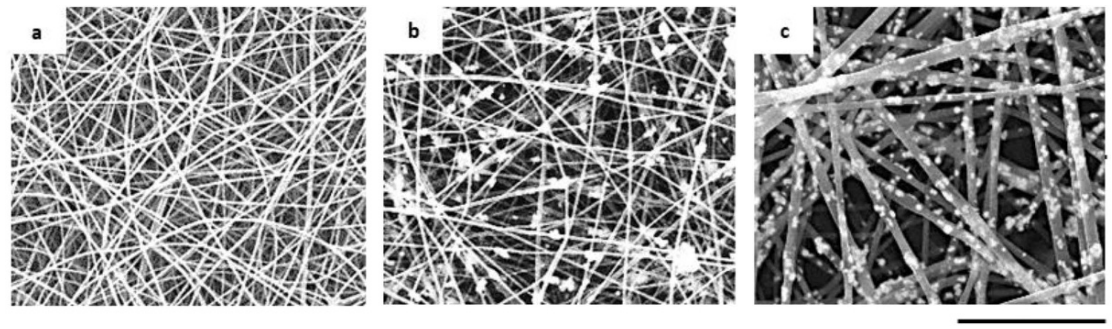

Figure 3. Scanning electron microscopy images (scale bar = 10 μm) of electrospun mats: (a) GL (control); (b) GL/BTNPs 10 GA; (c) GL/BTNPs 30 GA.

GL/BTNPs 30 GA, respectively. An analysis of the diameter distribution is reported in figures 4(a)–(c). The histogram (figure 4(e)) shows a comparison between the dimension of the aggregates within GL/BTNPs 10 and GL/BTNPs 10 GA fibers. The presence of GA affected the dimension of BTNP aggregates by significantly decreasing (t-test statistical analysis, $p < 0.0001$) their size (704.8 ± 169.4 nm and 462.5 ± 136.1 nm for GL/BTNPs 10 and GL/BTNPs 10 GA, respectively).

3.2.2. FTIR-ATR spectroscopy.

The FTIR-ATR spectra are presented in figure 5(a). The GL spectrum of showed the characteristic absorption peaks of the amide A (N–H stretching vibration), amide I (C = O stretching bonds), amide II (bending of N–H groups and C–N stretching vibration) and amide III (C–N bond vibration -in plane), respectively at 3289 cm^{-1}, 1639 cm^{-1}, 1534 cm^{-1} and 1241 cm^{-1} (Del Gaudio *et al* 2013, Suderman *et al* 2018). Furthermore, the peak related to Si–O–Si bands (1201 cm^{-1} and 1083 cm^{-1}) and stretching of Si–OH (920 cm^{-1}) confirmed that the cross-linking process successfully occurred through GPTMS (Tonda-Turo *et al* 2013). The GL/BTNPs 10 GA and GL/BTNPs 30 GA spectra showed the same peaks found in the GL spectra. Nevertheless, some of them (amide I, amide II and Si–O–Si bands) were slightly shifted at, respectively, 1646 cm^{-1}, 1541 cm^{-1} and 1074 cm^{-1} for GL/BTNPs 10 GA and at 1647 cm^{-1}, 1543 cm^{-1} and 1071 cm^{-1} for GL/BTNPs 30 GA.

3.2.3. Thermogravimetric analysis.

The BTNP content in the mats was evaluated by TGA. The thermogravimetric curves of the samples (figure 5(b)) showed that at the end of the heating process the residual percentage weights were, respectively, 25.06%, 46.24% and 53.29% for GL, GL/BTNPs 10 GA and GL/BTNPs 30 GA. These results suggest that the nanoparticle contents were 20% (w/w) and 30% (w/w) for GL/BTNPs 10 GA and GL/BTNPs 30 GA, respectively. Moreover, from the TGA curves it was possible to identify two main events that occurred: (i) evaporation of the residual water in the membranes between about 50 °C and 100 °C; (ii) the degradation of GL due to hydrolysis and endothermal oxidation (Salles *et al* 2015). The latter occurred at about 200 °C, 220 °C and 240 °C respectively for GL, GL/BTNPs 10 GA and GL/BTNPs 30.

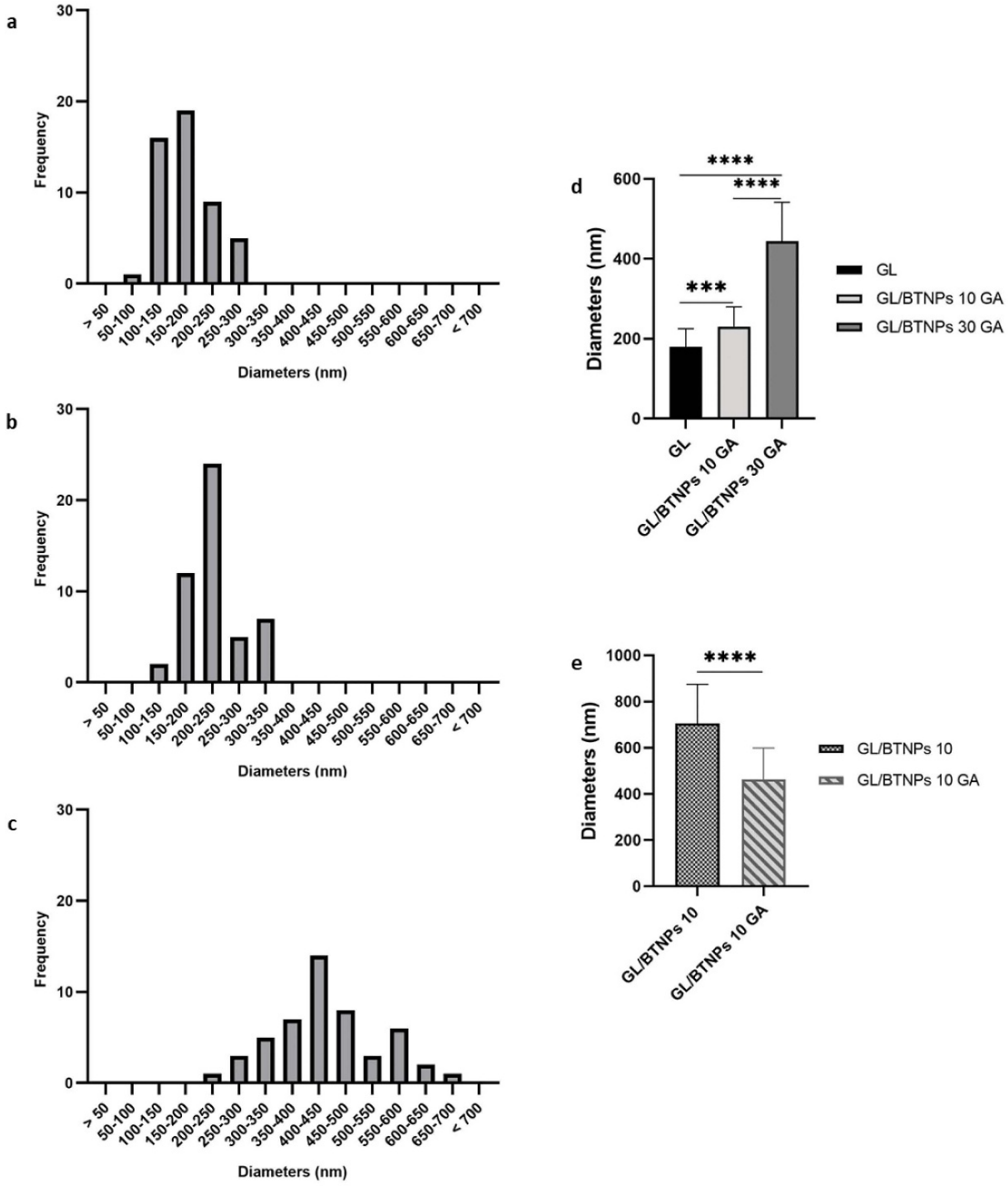

Figure 4. Morphological behavior of mats: diameter distribution of (a) GL, (b) GL/BTNPs 10 GA and (c) GL/BTNPs 30 GA fibers; (d) fiber diameters (statistical differences were identified with ordinary one-way ANOVA (***$p < 0.001$ and ****$p < 0.0001$)); (e) comparison between BTNP aggregates diameters on GL/BTNPs 10 and GL/BTNPs 10 GA (statistical differences were identified with a *t*-test (****$p < 0.0001$)).

3.2.4. Mechanical characterization.

Mechanical tensile properties of membranes were evaluated, and Young's modulus *E*, UTS and strain at failure are reported in figure 6. The stiffness of the samples increased with the increase in the amount of BTNPs in the mats ($E = 13.9 \pm 2.1$ MPa for GL, 32.42 ± 5.6 MPa for GL/BTNPs 10 GA and 46.6 ± 7.02 MPa for GL/BTNPs 30 GA; statistical analysis performed with ordinary one-way ANOVA, significative difference). Furthermore, the decrease of UTS (0.82 ± 0.02 MPa for GL, 0.40 ± 0.1 MPa for GL/BTNPs 10 GA and 0.45 ± 0.14 MPa for GL/BTNPs 30 GA) and ε% (8.11 ± 0.99% for GL, 1.92 ± 0.45% for GL/BTNPs 10 GA and 1.25 ± 0.22% for GL/BTNPs 30 GA) values were observed.

3.2.5. Cell tests.

The levels of viability of SaOS-2 cells on the GL-based membranes are reported in figure 7. No significant reduction of the ability of cells to convert non-fluorescent resazurin into a highly red fluorescent dye (resorufin) by cell metabolism was observed. Thus, the presence of BTNPs did not influence the viability of

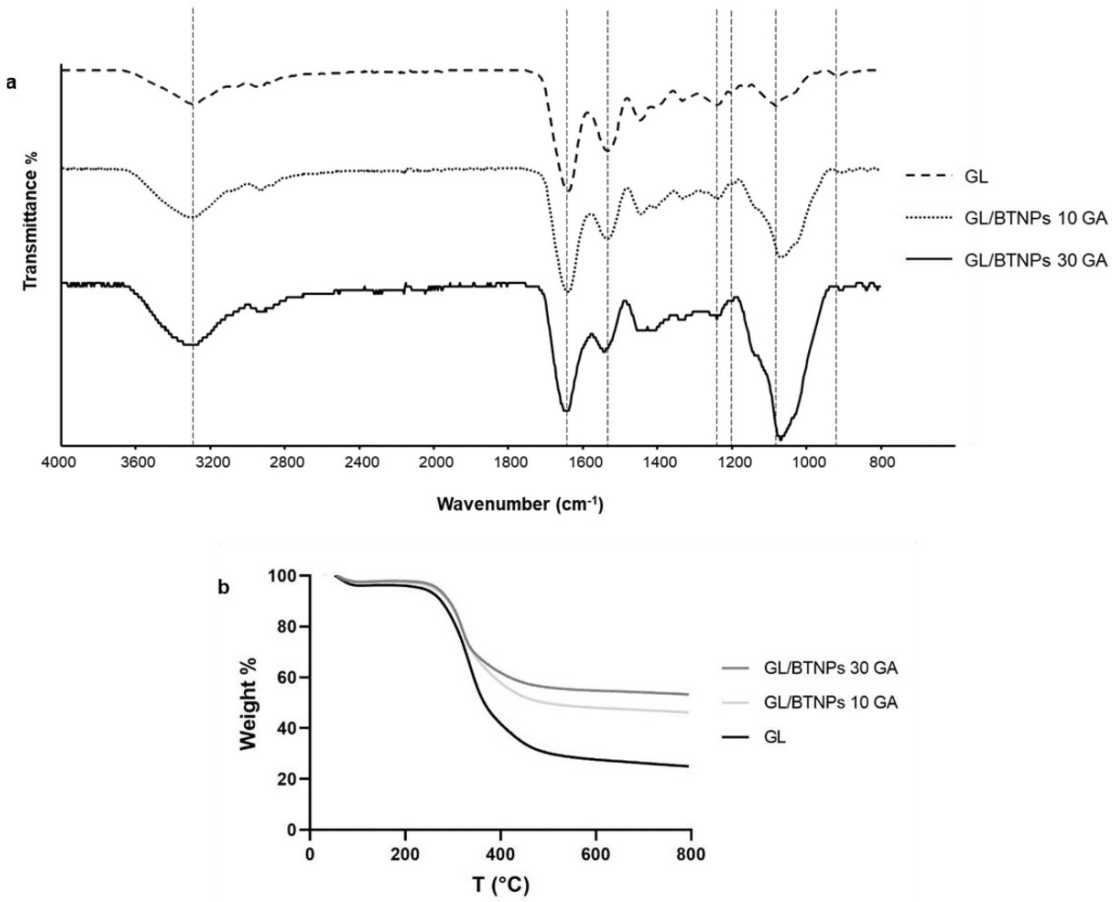

Figure 5. (a) FTIR-ATR spectra and (b) TGA of GL, GL/BTNPs 10 GA and GL/BTNPs 30 GA.

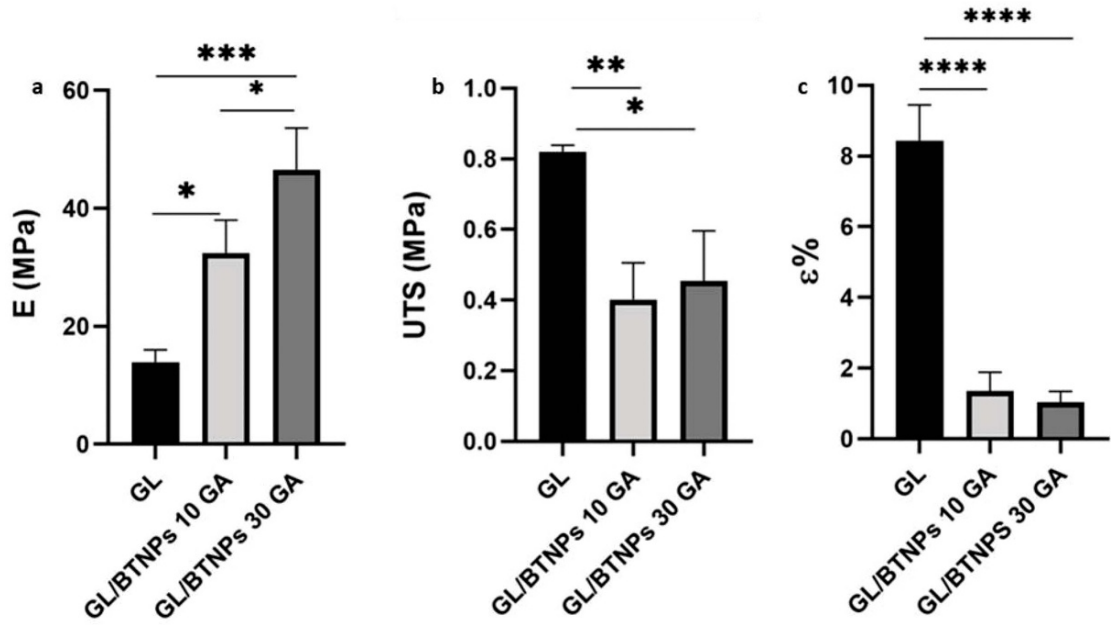

Figure 6. Mechanical behavior of membranes: (a) Young's modulus *E*, (b) UTS and (c) strain at failure (ε). Statistical differences were identified though ordinary one-way ANOVA ($^{*}p < 0.1$, $^{**}p < 0.01$, $^{***}p < 0.001$, $^{****}p < 0.0001$).

cells (no significative differences between GL and composite membranes). Concerning MSCs, ALP values revealed early osteogenic differentiation only on cells cultured on GL/BTNPs 30 GA, as the measured alkalization of GL/BTNPs 30 GA was double that of GL and GL/BTNPs 10 GA. Furthermore, calcium

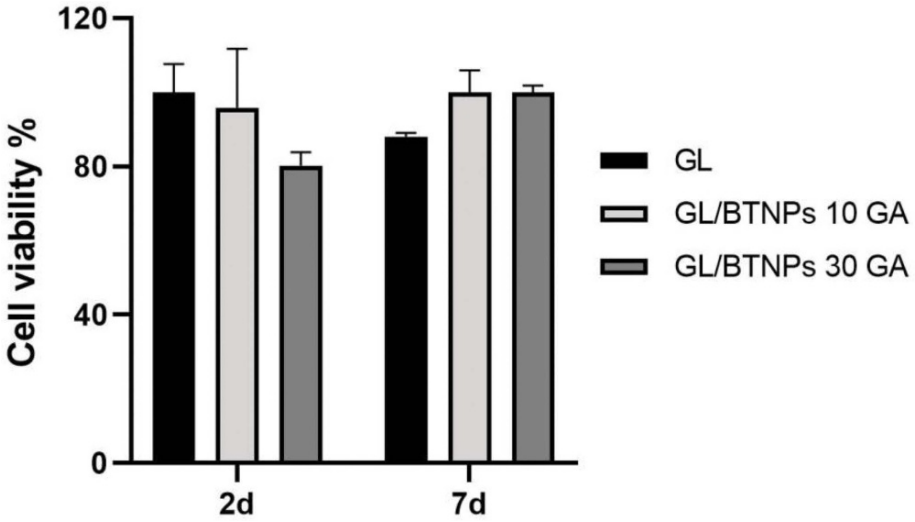

Figure 7. Evaluation of viability of SaOS-2 cells on GL, GL/BTNPs 10 GA and GL/BTNPs 30 GA at 2 and 7 d of culture.

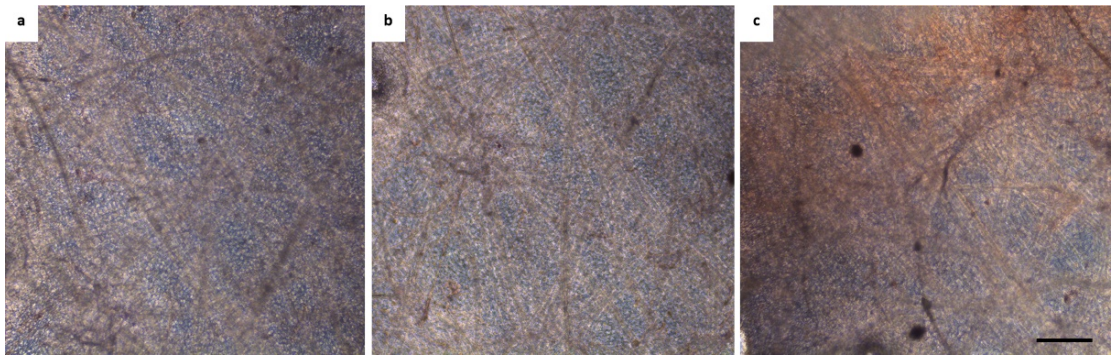

Figure 8. Representative images of alizarin red staining of MSCs after culture for 7 d on (a) GL, (b) GL/BTNPs 10 GA and (c) GL/BTNPs 30 GA. Scale bar = 50 μm.

deposition was slightly increased in GL/BTNPs 30 GA (figure 8(c)) compared with GL (figure 8(a)) and GL/BTNPs 10 GA (figure 8(b)). The formation of small nodules that were not detected in the other samples was in fact observed in GL/BTNPs .

4. Discussion

During the last two decades, the fabrication of nanocomposite materials that combine the advantageous features of both polymeric and active ceramic materials has been widely investigated for different applications (Carlberg *et al* 2007, Hanemann and Szabó 2010, Airimioaei *et al* 2016).

Here, a method for fabricating GL electrospun fibers loaded with piezoelectric BTNPs was proposed to combine the ECM-like composition of GL, the ECM-like structure obtained through electrospinning and the physiological-like piezoelectric behavior ascribed to BTNPs. A homogeneous distribution of BTNPs in scaffolds is required to guarantee the piezoelectric properties of composite scaffolds (Park *et al* 2012, Genchi and Ceseracciu *et al* 2016); however, SEM images of GL/BTNP samples (figure 1) showed a non-uniform distribution of the BTNPs in the fibers that appeared in the form of large aggregates. In order to improve the dispersion of nanoparticles in the fibers, GA was added to the initial BTNP solutions due to its well-known property as a nanoparticle stabilizer (Zhang *et al* 2009, Gao *et al* 2012, Alzahrani 2014, Ciofani *et al* 2014). To optimize the GA:BTNPs ratio, two different concentrations of GA were tested. The solution viscosity is a parameter which deeply affects the spinnability of the solution and consequently the feasibility of the electrospinning process (Subbiah *et al* 2005). The viscosity of the solution increased with increase in the GA concentration (figure 2(b)); the GL/BTNPs 30 GA 2:1 solution was too viscous ($\eta = 60$ Pa s) to obtain electrospun fibers. Therefore, the GA:BTNP weight ratio was set to 1:1. The influence of BTNPs on the morphological behavior of electrospun fibers was investigated (figure 3); a more uniform distribution of the

piezoelectric compounds in the fibers was observed. Indeed, the BTNPs appeared to be evenly distributed over the length of the GL/BTNPs 30 GA fibers (figure 3(c)). The increase in fiber size (statistical analysis performed with ordinary one-way ANOVA) was directly proportional to the BTNP content (figure 4(d)) and to the concomitant viscosity of the solution (Nezarati *et al* 2013, Gazquez *et al* 2017, Korycka *et al* 2018) as observed by rheological characterization. The actual reduction of the dimensions of the BTNP aggregates was demonstrated by comparing the aggregate diameters in the GL/BTNPs 10 and GL/BTNPs 10 GA membranes (figure 4(e)). EDX analysis (figure S4) confirmed the presence of Ba and Ti in the composite membranes and the values of weight and atomic percentage (table S1) confirmed the higher content of BTNPs in GL/BTNPs 30 GA with respect to GL/BTNPs 10 GA.

FTIR-ATR spectra of composite mats (figure 5(a)) showed the characteristic peaks of GL and GPTMS, confirming the absence of changes in the material structure and cross-linking due to BTNP loading. The shifting of peaks related to amide I, amide II and Si–O–Si bands could be attributed to the interaction between the polymeric compound and BTNPs, in accordance with Engin Sagirli *et al* (2016).

Furthermore, the amount of BTNPs in the composite membranes was detected by TGA. As expected, the BTNP content in the GL/BTNPs 30 GA mats was about 30% (w/w). On the contrary, the BTNP content in GL/BTNPs 10 GA was higher than expected [20% (w/w) when measured by TGA instead of 10% (w/w) loaded into GL solution]. This unexpected result was ascribed to the formation of aggregates during the spinning process and the incomplete homogeneous distribution of the BTNPs in the composite membranes. Therefore, the influence of BTNPs on the thermal degradation of GL was investigated. All the thermogravimetric curves (figure 5(b)) showed a similar trend but an increase in the degradation temperature of the composite membranes was observed; this shift demonstrates the good interaction of BTNPs with the GL matrix, thus enhancing chain entanglement (Mendes *et al* 2012).

The presence of BTNPs modified the mechanical properties of the scaffold, as composite membranes showed higher E than as-spun GL whereas a decrease of UTS and ε% was observed (Genchi and Ceseracciu *et al* 2016). The increase in the mechanical properties of PCL/BTNP substrates was previously reported by Baghi *et al* (2014).

The biocompatibility of the selected BTNPs was previously proved by several authors. Indeed, composite scaffolds of barium titanate/akermanite ceramics were preparated by Shokrollahi *et al* (2017). They did not record any toxic effect of the composite substrate on human bone marrow MSCs. Recently, Liu *et al* demonstrated that PCL/BTNP scaffolds do not affect the viability of MG63 osteoblast-like cells (2019). Random and aligned electrospun PLLA/BTNP mats were fabricated by Li *et al* (2017). The composite fibrous membranes in a random configuration promoted the spreading and osteogenic differentiation of bone marrow MSCs (Li *et al* 2017). In this work, the cytocompatibility of composite nanofibers was evaluated by performing resazurine assay. The histogram in figure 7 shows that no reduction in vitality was detected (no significative differences between the cell viability on the different substrates at several time points), demostrating that the presence of BTNPs in the fibers does not induce toxic effects on the SaOS-2 cells. Finally, the effect of piezoeletric particles on osteogenic differentiation was assessed on MSCs. Higher amounts of BTNPs reveal an early osteogenic differentiation effect and higher alkalinization compared with lower amounts of BTNPs and control conditions. Previous works confirmed an increase mineral deposits in MSCs cultured on piezoelectric substrates (Sobreiro-Almeida *et al* 2017) and incubated with BTNPs (Rocca *et al* 2015).

5. Conclusions

In this work a method for fabricating ECM-like GL/BTNP electrospun membranes was proposed. A uniform distribution of BTNPs in the composite fibers was obtained by dispersing GA in the initial solution. The fiber diameter increased with increase in the BTNP content. The presence of piezoelectric agents was confirmed by EDX and TGA analysis. The FTIR-ATR spectra of the membranes did not highlight any changes in the composition and cross-linking of the membranes. On the contrary, the mechanical behavior was drastically affected by the presence of ceramic nanoparticles. Finally, preliminary *in vitro* cell tests were performed to investigate the applicability of these scaffolds in tissue engineering.

Acknowledgments

The authors acknowledge Professor Marco Sangermano (Department of Applied Science and Technology, Politecnico di Torino, Turin, Italy) for his support in the physico-chemical characterization of the electrospun membranes. This work was supported by Compagnia San Paolo.

ORCID iDs

Chiara Tonda-Turo https://orcid.org/0000-0002-2149-7533
Gianni Ciofani https://orcid.org/0000-0003-1192-3647

References

Airimioaei M *et al* 2016 Effect of particle size and volume fraction of $BaTiO_3$ powders on the functional properties of $BaTiO_3$/poly(ε-caprolactone) composites *Mater. Chem. Phys.* **182** 246–55
Akilbekova D *et al* 2018 Biocompatible scaffolds based on natural polymers for regenerative medicine *Int. J. Biol. Macromol.* **114** 324–33
Alzahrani E 2014 Gum arabic-coated magnetic nanoparticles for methylene blue removal *Int. J. Innovative Res. Sci. Eng. Technol.* **03** 15118–29
Bagchi A *et al* 2014 Perovskite ceramic nanoparticles in polymer composites for augmenting bone tissue regeneration. *Nanotechnology* **25** 485101
Baxter F R *et al* 2010 Electrically active bioceramics: a review of interfacial responses *Ann. Biomed. Eng.* **38** 2079–92
Beloti M M *et al* 2006 In vitro biocompatibility of a novel membrane of the composite poly(vinylidene-trifluoroethylene)/barium titanate *J. Biomed. Mater. Res.* **79A** 282–8
Carlberg B, Norberg J and Liu J 2007 Electrospun nano-fibrous polymer films with barium titanate nanoparticles for embedded capacitor applications *Proc. Electronic Components and Technology Conf.* pp 1019–26
Ciofani G *et al* 2014 Cytocompatibility evaluation of gum arabic-coated ultra-pure boron nitride nanotubes on human cells *Nanomedicine* **9** 773–88
Dubey A K, Ravikumar K and Basu B 2019 Perovskite ceramics as new-generation materials for orthopedic applications *Trans. Indian Inst. Met.* **72** 1999–2010
Dubey A K, Tripathi G and Basu B 2010 Characterization of hydroxyapatite-perovskite ($CaTiO_3$) composites: phase evaluation and cellular response *J. Biomed. Mater. Res.* B**95B** 320–9
Engin Sagirli F Z *et al* 2016 In-situ preparation and characterization of pyrrole and tert-butyl 1-pyrrole-carboxylate on barium titanate/poly(acrylonitrile-co-methylacrylate) nanoparticles *React. Funct. Polym.* **100** 1–11
Gao Z *et al* 2012 Efficient disentanglement of boron nitride nanotubes using water-soluble polysaccharides for protein immobilization *RSC Adv.* **2** 6200
Del Gaudio C *et al* 2013 Induction of angiogenesis using VEGF releasing genipin-crosslinked electrospun gelatin mats *Biomaterials* **34** 7754–65
Gazquez G C *et al* 2017 Influence of solution properties and process parameters on the formation and morphology of YSZ and NiO ceramic nanofibers by electrospinning *Nanomaterials* **7**
Genchi G G Marino A *et al* 2016 Barium titanate nanoparticles: promising multitasking vectors in nanomedicine *Nanotechnology* **27** 232001
Genchi G G Ceseracciu L *et al* 2016 P(VDF-TrFE)/$BaTiO_3$ nanoparticle composite films mediate piezoelectric stimulation and promote differentiation of SH-SY5Y neuroblastoma cells *Adv. Healthcare Mater.* **5** 1808–20
Gnavi S *et al* 2018 Combined influence of gelatin fibre topography and growth factors on cultured dorsal root ganglia neurons *Anat. Rec.* **301** 1668–77
Gupta K C *et al* 2014 Nanofibrous scaffolds in biomedical applications *Biomater. Res.* **18** 5
Hanemann T and Szabó D V 2010 Polymer-nanoparticle composites: from synthesis to modern applications *Materials* 3468–517
Hofmann S and Garcia-Fuentes M 2011 Bioactive scaffolds for the controlled formation of complex skeletal tissues *Regenerative Medicine and Tissue Engineering - Cells and Biomaterials* ed D Eberli (Rijeka: InTech)
Jones J R 2005 Scaffolds for tissue engineering *Biomaterials, Artificial Organs and Tissue Engineering* ed L L Hench and J R Jones (Cambridge: Woodhead) pp 201–14
Kesireddy V and Kasper F K 2016 Approaches for building bioactive elements into synthetic scaffolds for bone tissue engineering *J. Mater. Chem.* B **4** 6773–86
Korycka P *et al* 2018 Effect of electrospinning process variables on the size of polymer fibers and bead-on-string structures established with a 2 3 factorial design *Beilstein J. Nanotechnol.* **9** 2466–78
Langer R and Vacanti J P 1993 Tissue engineering *Science* **260** 920–6
Li Y *et al* 2017 Electroactive $BaTiO_3$ nanoparticle-functionalized fibrous scaffolds enhance osteogenic differentiation of mesenchymal stem cells *Int. J. Nanomed.* **12** 4007–18
Liu J *et al* 2019 An intelligent material for tissue reconstruction : the piezoelectric property of polycaprolactone/barium titanate composites *Mat. Lett.* **236** 686–9
Marino A *et al* 2015 Piezoelectric nanoparticle-assisted wireless neuronal stimulation *ACS Nano* **9** 7678–89
Marino A *et al* 2017 Gelatin/nanoceria nanocomposite fibers as antioxidant scaffolds for neuronal regeneration *Biochim. Biophys. Acta. Gen. Subj.* **1861** 386–95
Mendes S F *et al* 2012 Effect of filler size and concentration on the structure and properties of poly(vinylidene fluoride)/$BaTiO_3$ nanocomposites *J. Mater Sci.* **47** 1378–88
Nezarati R M, Eifert M B and Cosgriff-Hernandez E 2013 Effects of humidity and solution viscosity on electrospun fiber morphology *Tissue Eng.* C**19** 810–19
Ng R *et al* 2012 Three-dimensional fibrous scaffolds with microstructures and nanotextures for tissue engineering *RSC Adv.* **2** 10110
O'Brien F J 2011 Biomaterials & scaffolds for tissue engineering *Mater. Today* **14** 88–95
Paim Á *et al* 2018 Mesenchymal stem cell cultivation in electrospun scaffolds: mechanistic modeling for tissue engineering *J. Biol. Phys.* 245–71
Park K I *et al* 2012 Flexible nanocomposite generator made of BaTiO 3 nanoparticles and graphitic carbons *Adv. Mater.* **24** 2999–3004
Pezeshki-Modaress M, Zandi M and Rajabi S 2018 Tailoring the gelatin/chitosan electrospun scaffold for application in skin tissue engineering: an *in vitro* study *Prog. Biomater.* **7** 207–18
Rajabi A H, Jaffe M and Arinzeh T L 2015 Piezoelectric materials for tissue regeneration: a review *Acta. Biomater.* **24** 12–23
Rajabi M *et al* 2018 Fabrication and characterization of electrospun laminin-functionalized silk fibroin/poly(ethylene oxide) nanofibrous scaffolds for peripheral nerve regeneration *J. Biomed. Mater. Res.* B **106** 1595–604

Ravichandran R *et al* 2012 Advances in polymeric systems for tissue engineering and biomedical applications *Macromol. Biosci.* **12** 286–311

Rocca A *et al* 2015 Barium titanate nanoparticles and hypergravity stimulation improve differentiation of mesenchymal stem cells into osteoblasts *Int. J. Nanomed.* **10** 433–45

Salles T H C, Lombello C B and D'Ávila M A 2015 Electrospinning of gelatin/poly (vinyl pyrrolidone) blends from water/acetic acid solutions *Mater. Res.* **18** 509–18

Sell S A *et al* 2010 The use of natural polymers in tissue engineering: a focus on electrospun extracellular matrix analogues *Polymers* **2** 522–53

Shokrollahi H, Salimi F and Doostmohammadi A 2017 The fabrication and characterization of barium titanate/akermanite nano-bio-ceramic with a suitable piezoelectric coe ffi cient for bone defect recovery *J. Mech. Behav. Biomed. Mater.* **74** 365–70

Sisson K *et al* 2010 'Fiber diameters control osteoblastic cell migration and differentiation in electrospun gelatin' *J. Biomed. Mater. Res.* A **94A** 1312–20

Sobreiro-Almeidao *et al* 2017 Human mesenchymal stem cells growth and osteogenic differentiation on piezoelectric poly(vinylidene fluoride) microsphere substrates *Int. J. Mol. Sci.* **18** 2391

Subbiah T *et al* 2005 Electrospinning of nanofibers *J. Appl. Polym. Sci.* **96** 557–69

Suderman N, Isa M I N and Sarbon N M 2018 Characterization on the mechanical and physical properties of chicken skin gelatin films in comparison to mammalian gelatin films *IOP Conf. Series: Materials Science and Engineering* (Bristol: Institute of Physics Publishing.)

Tonda-Turo C *et al* 2013 Crosslinked gelatin nanofibres: preparation, characterisation and *in vitro* studies using glial-like cells *Mater. Sci. Eng.* C **33** 2723–35

Vasita R and Katti D S 2006 Nanofibers and their applications in tissue engineering *Int. J. Nanomed.* **1** 15–30

Wen J and Liu M 2014 Piezoelectric ceramic (PZT) modulates axonal guidance growth of rat cortical neurons via RhoA, Rac1, and Cdc42 pathways *J. Mol. Neurosci.* **52** 323–30

Zhang L *et al* 2009 Gum arabic-coated magnetic nanoparticles for potential application in simultaneous magnetic targeting and tumor imaging *AAPS J.* **11** 693